Ru^{II} Complexes of Bis(1,10-phenanthrolin-2-yl)diazines

Darren Brown,[a] Ruifa Zong,[a] and Randolph P. Thummel*[a]

Keywords: Bridging ligands / Ruthenium / Phenanthrolines / Diazines

A series of three bis-tridentate bridging ligands has been prepared in which two 1,10-phenanthroline units have been symmetrically appended to a central pyridazine, pyrimidine, or pyrazine ring. These ligands have been treated with [Ru(tpy-d_{11})Cl_3] to afford both mono- and dinuclear complexes whose photo- and electrochemical properties have been evaluated (tpy = 2,2′:6′,2′′-terpyridine). A structural comparison is made between [(tpy)Ru(**3**)Ru(tpy)]$(PF_6)_4$ and a previously reported complex involving 2,2′-bipyridines in place of phenanthrolines on the bridging ligand and surprisingly little difference is found.

Lehn and co-workers have constructed an elegant series of bis-terdentate ligands (**1**) based on a central pyrimidine ring with the intent of using these systems as bridging ligands for the formation of rack-type polynuclear complexes.[1] An important aspect of constructing such rack systems is the ability to arrange the bridging units in a parallel array to preserve a rectangular rack.[2] They found that the spatial relationship between two bound Ru(tpy) units was governed by the nature of the central substituent R, which was varied between hydrogen, methyl, phenyl, and 9-anthracenyl. When R = H, the planes of the two Ru-bound terpyridines defined a convergence angle of 36.3°, where a parallel arrangement (angle = 0°) was desired for optimum rack formation. This deformation results from a pinching of the ligand which causes the two outer pyridine groups to move closer to one another. We reasoned that further constraining the ligating portion of the system by substituting 1,10-phenanthroline (phen) for the 2,2′-bipyridine (bpy) subunits might offset this pinching effect and result in a more parallel arrayed system.

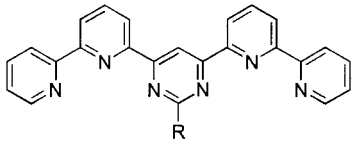

1

In an earlier work we have reported the preparation and Ru^{II} complexation of a series of diphen-substituted diazines **2**−**4**.[3] All three ligands formed mononuclear heteroleptic complexes [Ru(tpy-d_{11})(L)]$^{2+}$ (tpy-d_{11} = perdeuterio-2,2′:6′,2′′-terpyridine), while **3** and **4** also formed dinuclear complexes [(tpy-d_{11})Ru(L)Ru(tpy-d_{11})]$^{4+}$. The use of tpy-d_{11} in place of the protio-analogue greatly facilitated analysis of the NMR spectra. The chemical shifts of the protons on the central pyrimidine or pyrazine ring indicated that these resonances were consistent with the additivity of deshielding effects due to the attached phens with shielding effects from the coordinated tpys. In this paper we report on the structural properties of [(tpy)Ru(**3**)Ru(tpy)]$^{4+}$, as well as on the electronic and photophysical properties of the Ru^{II} complexes of **2**−**4**.

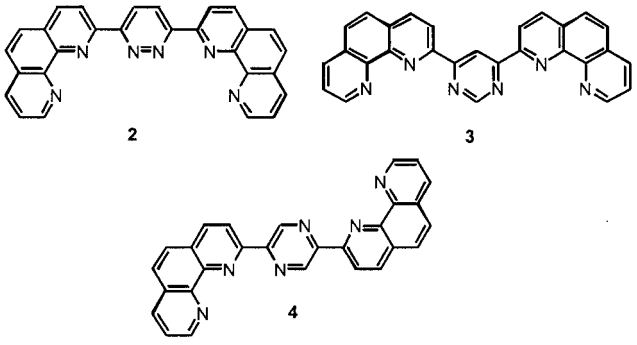

2 **3** **4**

A crystal of [(tpy)Ru(**3**)Ru(tpy)]$(PF_6)_4$ suitable for X-ray analysis was grown from acetonitrile/acetone. In this instance the use of protio-tpy as the auxiliary ligand was preferred. An ORTEP plot showing the structure of the cation is illustrated in Figure 1, and selected structural data is summarized in Table 1 along with the corresponding data from the reported structure for [(tpy)Ru(**1**)Ru(tpy)]$(PF_6)_4$, where R=H.[1] We were quite surprised by the close similarity of the two structures. The central benzo-ring of the phen subunits in **3** pulls C5 and C8 closer by 0.20 Å, and this may straighten out the ligand somewhat. However, this

[a] Department of Chemistry, 136 Fleming Building, University of Houston,
Houston, Texas 77204-5003, USA

change is more than compensated by a lengthening of the C10−C17 bond. The bond angles beyond the chelate rings are found to decrease on the phen side of **3** by about 4.2°, while they increase on the side that pyrazine is coordinated by 1.9°. The overall pinching angle of the molecule actually increases from 25.6° to 30.8° in the complex of **3**. These changes in ligand geometry in going from **1** to **3** are moderated by small adjustments in the Ru−N bond lengths - the Ru−N12 distance is shortened by 0.013 Å and Ru−N15 by 0.015 Å so that the convergence angle remains essentially the same.

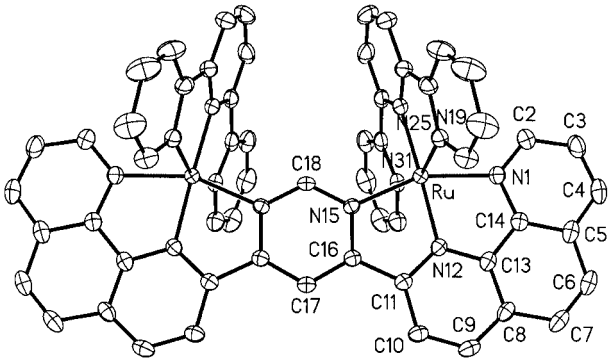

Figure 1. ORTEP diagram of the cation of [(tpy)Ru(**3**)Ru(tpy)]$(PF_6)_4$ with atomic numbering scheme

Table 1. Selected geometric features [bond lengths (Å) and angles (°)] of [(tpy)Ru(**3**)Ru(tpy)]$(PF_6)_4$ compared with analogous features of [(tpy)Ru(**1**)Ru(tpy)]$(PF_6)_4$

	Bridging ligand[a]	
	3	**1**
Ru−N1	2.092(3)	2.090(5)
Ru−N12	1.975(3)	1.988(5)
Ru−N15	2.069(3)	2.084(4)
Ru−N19	2.075(3)	2.090(5)
Ru−N25	1.992(3)	1.993(5)
Ru−N31	2.083(3)	2.092(5)
Ru−Ru	6.0583(5)	6.160
C5−C8	2.863(5)	3.063(10)
C10−C17	3.147(4)	3.075(8)
C28−C28′	3.350(7)	3.405(11)
<C5−C14−C13	119.2(3)	123.5(6)
<C8−C13−C14	122.9(3)	127.1(5)
<C10−C11−C16	129.2(3)	127.3(5)
<C11−C16−C17	125.4(3)	123.5(5)
Convergence angle	36.2	36.3
Pinching angle	30.8	25.6
Bending angle	164.7	170.3

[a] Numbering pattern from Figure 1 with the same relative atom positions for both complexes.

It is interesting to note that the bridging ligand is slightly bent in both complexes, with a larger bend for the complex of **3**. Figure 2 shows how this relatively small deformation is amplified by the tpy ligands which are splayed much farther apart on one side of the complex. On the closer side, the carbon atoms C34 and C34′ are separated by 3.55 Å, while C28 and C28′ are 3.35 Å apart so that some π-stacking effects may be important. On the further side, C22 and C22′ are separated by 7.73 Å. In the complex of **1**, the "open" side of tpy is occupied by a molecule of acetone solvent; this feature is not observed for the complex of **3**. However, the crystal packings are remarkably similar in both cases. It appears that the distortions from ideal octahedral geometry around Ru^{II} caused by tridentate complexation with tpy dictate the shape of the complex, and these effects cannot be greatly influenced by structural modification of the bridging bis-tridentate moiety. The ability of these ligands to participate in rack-type polynuclear structures involving octahedral centers is therefore somewhat compromised.

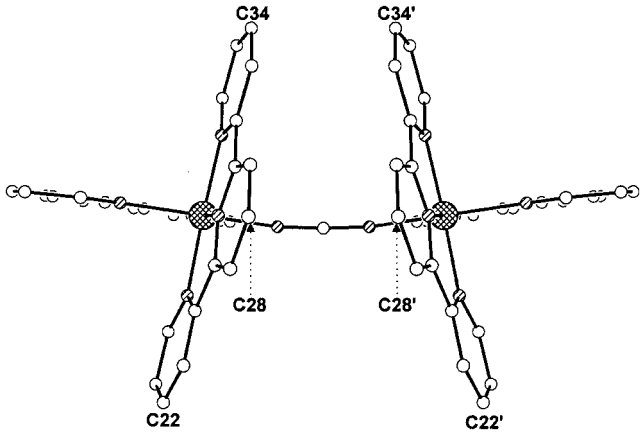

Figure 2. Side view of the cation of [(tpy)Ru(**3**)Ru(tpy)]$(PF_6)_4$

The electronic absorption and emission properties of the mono- and dinuclear complexes of **2**−**4** are summarized in Table 2, and the spectra involving **3** and **4** are illustrated in Figure 3. The mono- and dinuclear complexes all show long wavelength absorption bands that may be attributed to a metal-to-ligand charge-transfer (MLCT) state typically associated with such Ru^{II} polypyridine complexes.[4] This state involves the photoexcitation of an electron from the HOMO, which is a metal-centered d orbital, to the LUMO, which is a π*-orbital localized on one of the ligands. In the cases of the heteroleptic mononuclear complexes of **2**−**4**, the MLCT state consists of two components, one involving the more electronegative and more delocalized bridging diazine and the other involving the tpy-d_{11} ligand. This latter component shows a fairly consistent absorption at higher energy (445−451 nm), reflecting the higher energy of the π*-state for tpy. The lower energy component involving the diazine decreases in energy in the order **2** (522 nm), **4** (530 nm), **3** (538 nm). The energy difference may partly be associated with the disposition of the uncoordinated phen ring. For the complex of **3**, this ring is relatively unhindered in either planar conformation, while the complexes of **4** and **2** show increasing steric hindrance to ligand planarity. The allowed transitions also follows the same trend as can be seen by looking at the ratios of the molar absorptivities for

Table 2. Photophysical and electrochemical data for Ru^{II} complexes

Complex	Absorption[a] λmax, nm (ε, $M^{-1}\cdot cm^{-1}$)	Emission[a] λ_{em}, nm	Φ≅[c]	$E_{1/2}$[b], V OX	RED
$[Ru(\mathbf{2})(tpy\text{-}d_{11})]^{2+}$	522 (6780), 445 (10580)	737	2.9×10^{-3}	+1.38	−0.84, −1.26, −1.62
$[Ru(\mathbf{3})(tpy\text{-}d_{11})]^{2+}$	538 (11500), 451 (9660)	751	3.1×10^{-3}	+1.40	−0.72, −1.20, −1.60
$[Ru(\mathbf{4})(tpy\text{-}d_{11}]^{2+}$	530 (5950), 451 (6470)	744	3.0×10^{-3}	+1.40	−0.74, −1.18, −1.55
$[(tpy\text{-}d_{11})Ru(\mathbf{3})Ru(tpy\text{-}d_{11})]^{4+}$	647 (10500), 569 (10360) 444 (24040)	842	2.4×10^{-5}	+1.38, +1.56	−0.33, −0.83, −1.56
$[(tpy\text{-}d_{11})Ru(\mathbf{4})Ru(tpy\text{-}d_{11})]^{4+}$	636 (15300), 586sh (6010), 447 (14520)	839	1.1×10^{-4}	+1.36, +1.56	−0.35, −0.76, −1.37

[a] 5×10^{-5} M in CH3CN at 25 °C. [b] Solutions were 0.1 M TBAP in CH_3CN; the sweep rate was 200 mV/s. [c] Referenced to $[Ru(bpy)_3]Cl_2$ in air-equilibrated water (Φ = 0.028).

the two bands for each mononuclear complex. The ratio of the molar absorptivities for the MLCT bands for the tpy vs. the diazine moiety is 1.56 for the complex of **2**, 1.09 for **4**, and 0.84 for **3** which is the most planar.

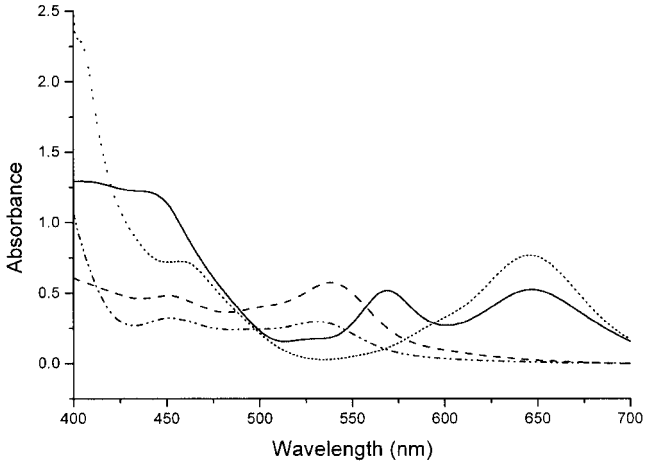

Figure 3. Electronic absorption spectra for Ru^{II} complexes of **3** and **4** in CH_3CN (5×10^{-5} M): $[Ru(\mathbf{3})(tpy\text{-}d_{11})]^{2+}$ (— —), $[Ru(\mathbf{4})(tpy\text{-}d_{11})]^{2+}$ (·· —·· —), $[(tpy\text{-}d_{11})Ru(\mathbf{3})Ru(tpy\text{-}d_{11})]^{4+}$ (—), $[(tpy\text{-}d_{11})Ru(\mathbf{4})Ru(tpy\text{-}d_{11})]^{4+}$ (····)

The dinuclear complexes of **3** and **4** both show enhanced MLCT bands associated with the two auxiliary tpy-d_{11} ligands that are very roughly double their mononuclear counterparts. The longer wavelength components are shifted to much lower energies, hence, the color is green. As has been observed earlier for other diazine-bridged dinuclear Ru^{II} complexes,[4] two bands are seen at longer wavelength. The spectrum for the pyrimidine system shows bands at 647 and 569 nm, whereas that of the pyrazine system shows a strong band at 636 with a shoulder at 586 nm.

All five complexes show weak to medium emission bands when excited at their long wavelength absorption maximum. These emissions follow the expected trend based on the absorptions of the mononuclear complex so that the Stokes shifts remain almost constant at 213−215 nm. The dinuclear complexes show weaker emissions at lower energies, which may be due to quenching by the second metal center.

The redox properties are also consistent and well behaved (reported in Table 2). All five complexes show metal-based Ru^{II}/Ru^{III} oxidations in the range of 1.36−1.40 V. For the dinuclear complexes a second wave at 1.56 V is observed for oxidation of the second metal. This second wave is separated by 0.18−0.20 V from the first wave, indicating a strong interaction between the two metal centers. As observed previously, the interaction is stronger when the metal centers communicate through a pyrazine as opposed to a pyrimidine bridge. Reductions are typically ligand based. For the mononuclear complexes, the first two reductions lie in the range of −0.72 to −0.84 V and −1.18 to −1.26 V, and are associated with the complexed diphen−diazine ligand. The third reduction for these systems is assigned to the tpy-d_{11} ligand (−1.55 to −1.62 V). For the dinuclear complexes, complexation by a second metal increases the reduction potentials associated with the bridging diazine ligand by about +0.4 V.

Experimental Section

The preparation of the ligands **2−4** and their Ru^{II} complexes has been reported.[3] Electronic spectra were obtained on a Perkin−Elmer Lambda 3B spectrophotometer. Emission spectra were obtained on a Perkin−Elmer LS-50 luminescence spectrometer. Cyclic voltammetry was carried out in a conventional three-electrode cell with a BAS-27 voltammeter and a Houston Instruments model 100 X-Y recorder according to a previously described procedure.[5]

X-ray Determination: All measurements were made with a Siemens SMART platform diffractometer equipped with a 1 K CCD area detector. A hemisphere of data (1271 frames at 5 cm detector distance) was collected using a narrow-frame method with scan widths of 0.30° in omega and an exposure time of 30 s/frame. The first 50 frames were remeasured at the end of data collection to monitor instrument and crystal stability, and the maximum correction on I was <1%. The data were integrated using the Siemens SAINT program, and the intensities corrected for Lorentz factor, polarization, air absorption, and absorption due to variation in the path length through the detector faceplate. A psi scan absorption correction was applied based on the entire data set. Redundant reflections were averaged. Final cell constants were refined using 3854 reflections having $I > 10\sigma(I)$, and these, along with other information pertinent to data collection and refinement, are listed in Table 3. The Laue symmetry was determined to be mmm, and from the

systematic absences noted, the space group was shown to be either *Pna*2(1) or *Pnma*. The asymmetric unit consists of one-half of the Ru_2 tetracation situated about a mirror plane, one PF_6 anion in a general position, two half PF_6 anions situated on mirror planes, a solvent molecule of acetone in a general position, and one-half molecule of acetonitrile on a mirror plane. One of the anions and the acetone are disordered over two slightly different orientations. The acetone had to be treated as an ideal rigid body in order to facilitate refinement. Additionally, the hydrogens on acetonitrile are disordered.

Table 3. Crystallographic data for $[(tpy)Ru(\mathbf{3})Ru(tpy)](PF_6)_4 \cdot 2C_3H_6O \cdot CH_3CN$

Empirical formula	$C_{66}H_{53}F_{24}N_{13}O_2P_4Ru_2$
a, Å	16.0569(10)
b, Å	24.8957(15)
c, Å	17.7269(11)
α, °	90.00
β, °	90.00
γ, °	90.00
V, Å^3	7086.3(8)
Z	4
Molecular weight	1842.23
Space group	*Pnma*
T, °C	−50
λ, Å	0.71073
$\rho_{calcd.}$, g cm^{-3}	1.727
μ, mm^{-1}	0.636
$R_1 = \Sigma\|\|F_o\| - \|F_c\|\|/\Sigma\|F_o\|$	0.0346
$wR_2 = \{[\Sigma[w(F_o^2 - F_c^2)^2]/\Sigma[w(F_o^2)^2]\}^{1/2}$	0.0928
$w = [\sigma^2(F_o^2) + (0.0525P)^2 + (18.5276P)]^{-1}$, where $P = (F_o^2 + 2F_c^2)/3$	

Acknowledgments

We would like to thank the Division of Chemical Sciences, Office of Basic Energy Sciences, U. S. Department of Energy (Contract No. DE-FG03−02ER15334) and the Robert A. Welch Foundation (E-621) for financial support of this work. We also thank Dr. James Korp for assistance with the X-ray determination which required the use of MRSEC/TCSUH Shared Experimental Facilities supported by the National Science Foundation under Award Number DMR-9632667 and the Texas Center for Superconductivity at the University of Houston.

[1] [1a] G. S. Hanan, C. R. Arana, J.-M. Lehn, D. Fenske, *Angew. Chem. Int. Ed. Engl.* **1995**, *34*, 1122−1124. [1b] G. S. Hanan, C. R. Arana, J.-M. Lehn, G. Baum, D. Fenske, *Chem. Eur. J.* **1996**, *2*, 1292−1302.

[2] [2a] S. Leininger, B. Olenyuk, P. J. Stang, *Chem. Rev.* **2000**, *100*, 853−908. [2b] G. F. Swiegers, T. Malefetse, *Chem. Rev.* **2000**, *100*, 3483−3537. [2c] V. Amendola, L. Fabbrizzi, P. Pallavicini, *Coord. Chem. Rev.* **2001**, *216−217*, 435−448. [2d] P. N. W. Baxter, R. G. Khoury, J.-M. Lehn, G. Baum, D. Fenske, *Chem. Eur. J.* **2000**, *6*, 4140−4148. [2e] L. M. Greig, D. Philp, *Chem. Soc. Rev.* **2001**, *30*, 287−302. [2f] T. Bark, M. Düggeli, H. Stoeckli-Evans, A. von Zelewsky, *Angew. Chem. Int. Ed.* **2001**, *40*, 2848−2851.

[3] D. Brown, S. Muranjan, Y. Jang, R. Thummel, *Org. Lett.* **2002**, *4*, 1253−1256.

[4] D. Brown, S. Muranjan, R. P. Thummel, *Eur. J. Inorg. Chem.* **2003**, 3547−3553.

[5] V. Goulle, R. P. Thummel, *Inorg. Chem.* **1990**, *29*, 1767−1772.

Received February 19, 2004
Early View Article
Published Online June 7, 2004

